Fast-Response Fiber-Optic FPI Temperature Sensing System Based on Modulated Grating Y-Branch Tunable Laser

Yang CHEUNG[1], Zhenguo JING[1*], Qiang LIU[3], Ang LI[2], Yueying LIU[2], Yihang GUO[2], Sen ZHANG[2], Dapeng ZHOU[1], and Wei PENG[1]

[1]*School of Physics, Dalian University of Technology, Dalian 116024, China*

[2]*School of Optoelectronic Engineering and Instrumentation Science, Dalian University of Technology, Dalian 116024, China*

[3]*School of Computer and Electronic Information / School of Artificial Intelligence, Nanjing Normal University*, *Nanjing 210023, China*

[*]Corresponding author: Zhenguo JING E-mail: jingzg@dlut.edu.cn

Abstract: In this paper, a cost-effective and miniaturized instrument is proposed, which is based on a tunable modulated grating Y-branch (MG-Y) laser for rapid temperature measurement using a Fabry-Perot interferometer (FPI) sensor. The FPI sensor with a 1463-μm cavity length is a short segment of a capillary tube sandwiched by two sections of single-mode fibers (SMFs). This system has a broad tunable range (1527 nm–1567 nm) with a wavelength interval of 8 pm and a tuning rate of 100 Hz. Temperature sensing experiments are carried out to investigate the performance of the system by demodulating the absolute cavity length of the FPI sensor using a cross-correlation algorithm. Experimental results show that the sensor can reach the response time as short as 94 ms with the sensitivity of 802 pm/℃. Benefiting from the homemade and integrated essential electrical circuits, the entire system has the small size, low cost, and practical application potential to be used in the harsh environment for rapid temperature measurement.

Keywords: MG-Y laser; interrogator; rapid temperature measurement; cross-correlation algorithm

Citation: Yang CHEUNG, Zhenguo JING, Qiang LIU, Ang LI, Yueying LIU, Yihang GUO, *et al.*, "Fast-Response Fiber-Optic FPI Temperature Sensing System Based on Modulated Grating Y-Branch Tunable Laser," *Photonic Sensors*, 2024, 14(1): 240125.

1. Introduction

A temperature, a vital sign used to monitor the function of the equipment, is an essential indicator of equipment health and operation status [1–4]. Early fault detection is critical to avoid system failures. And condition monitoring systems must have the ability to detect sudden deterioration, so there is sufficient time to intervene appropriately before a major failure [5]. In addition, monitoring and exploration of seawater are becoming increasingly important, the water temperature is one of the fundamental parameters of ocean measurement, and timely and accurate acquisition of the seawater temperature is important for fisheries, disaster warnings, and military security [6–8]. The seawater mass boundaries are superimposed on each other, and temperature gradients exist at different levels, so the sensitivity and response time of the sensors must be considered when using the ocean sensors to measure seawater temperatures [9, 10]. Traditional test methods typically use electronic

Received: 29 January 2023 / Revised: 1 June 2023

DOI: 10.1007/s13320-023-0690-0
Article type: Regular

sensors to assess the condition of the equipment. However, these methods have significant drawbacks in terms of real-time measurement due to the strong electromagnetic interference or slow speed [11]. Fiber Bragg grating (FBG) sensors have been widely used for rapid temperature detection due to their unique advantages of the high sensitivity, electromagnetic immunity, and suitability for embedment. But the fabrication of the FBG requires the complex and expensive equipment, and the sensing length is quite long, typically up to 10 mm, which leads to the relatively low spatial resolution [12], limiting their practical applications [13–15]. Optic-fiber Fabry-Perot interferometer (FPI) sensors can overcome these shortcomings, which can be fabricated with a very short length to provide better spatial resolution and can also be used to measure temperatures with short response time [16–18]. The all-fiber FPI sensor manufactured by fusion splicing a short section of a capillary between two standard single-mode fibers (SMFs) has attracted extensive attention [19–21], because its fabrication procedure is relatively simple, and its temperature response time is within 100 ms [22], which meets most of the requirements for rapid temperature measurement [16].

When the ambient temperature around the FPI sensor changes, the cavity length of the sensor varies. By measuring the corresponding changes in the intensity or phase of the interference signals, the transient temperature variations can be monitored. The intensity demodulation scheme is simple and easy to operate, but the dynamic range is limited. In addition, the intensity demodulation technique is prone to the error induced by external environmental noise [22]. Spectral interrogation is the most commonly used method for phase demodulation, which is able to obtain the absolute cavity length with the sub-nanometer resolution [23, 24]. Given the need to improve the temperature measurement accuracy, precise acquisition of the real-time interference spectrum is a key requirement. One of the most straightforward methods is to acquire the spectrum by using a commercial spectrometer, but its high-cost and low-speed characteristics make it impossible to be used for most in situ measurement [25]. Alternatively, the method using an electrically tunable FP filter [26] has been extensively studied because of some remarkable advantages, such as the compact and in-field measurement, which is more widely used in field applications than the method mentioned above. Nevertheless, the nonlinearity and non-repeatability of the tunable piezoelectric ceramic driving process of the tunable FP filter could lead to minor system errors [27]. The techniques mentioned above have some drawbacks, such as high costs and strict operating conditions. Hence, an alternative low-cost and integrated high-speed FPI demodulation system is needed for rapid temperature measurement.

In recent years, the use of tunable lasers to obtain the interference spectrum of the interferometer has received extensive attention [27–29]. Measurement systems that involve fiber lasers have the advantages of an extensive tuning range and high coupling efficiency. However, fiber lasers are usually expensive and have a slow tuning rate which is restricted by the core component, such as tunable fiber filters [30]. The vertical cavity surface emitting laser (VCSEL) and external cavity semiconductor laser (ECSL) comprise micromechanical components, which leads to poor mechanical resistance, limiting their applications [31]. The modulated grating Y-branch (MG-Y) laser is developed for telecommunication applications, which is regarded as a promising wavelength-tunable laser due to its extensive wavelength tuning range (>40 nm), fast wavelength switching speed (<10 ns), and compact size without mechanical moving parts [27, 32]. Its high-speed switching, linear scanning, and narrow linewidth properties are very useful in various fiber sensing applications. However, for telecommunication applications, the wavelength of MG-Y lasers is typically tuned with the coverage of the entire C-band with the 50 GHz spacing. This wide

wavelength spacing prevents the MG-Y laser from the applications in the sensing field due to the limited measurement accuracy; therefore, it is desired to develop a narrow-spaced wavelength tuning technique for the MG-Y lasers to be applied to the fiber-optic sensing field.

In view of the practical considerations described above, a cost-effective and high-speed optical fiber FPI temperature measurement system using an MG-Y laser is proposed in this work. An MG-Y laser is adopted as the tunable laser source in this system. The laser drive circuit, temperature control circuit, and signal detection circuit are developed and integrated as a stand-alone instrument. Firstly, the rapid temperature measurement principle based on the FPI sensor and wavelength tuning mechanism of the MG-Y laser is introduced. Then, the development details and functional validation are described. Finally, rapid temperature experiments are carried out, and the system performance is demonstrated.

2. Principle of FPI sensor for rapid temperature measurement

The schematic diagram of the proposed fiber-optic FPI sensor for the temperature measurement is shown in Fig. 1. The sensor consists of a hollow capillary tube and two sections of single-mode fibers. There are two interfaces in the FPI structure: one is the interface between SMF1 and the hollow capillary tube, and the other is the interface between the hollow capillary tube and SMF2. When the reflectivity of two surfaces of the FPI sensor is low ($R<4\%$), the multiple-beam interference can be simplified as the two-beam interference [29]. The reflection light intensity I_R can be expressed as follows:

$$I_R = A + B\cos(4n\pi L/\lambda + \pi) \tag{1}$$

where A is the direct current (DC) component of the interferometric fringe, B is the fringe visibility, and λ is the wavelength, n is the refractive index of the FPI sensor, and L is the initial cavity length. The length of the hollow capillary tube changes significantly when the ambient temperature varies around the FPI sensor. The hollow capillary tube exhibits a low coefficient of the thermal expansion similar to that of silica, which is about $\alpha_c = 5.5\times10^{-7}$ ℃. Correspondingly, the change in the cavity length ΔL due to the temperature variation ΔT can be expressed as

$$\Delta L = L\alpha_c\Delta T \tag{2}$$

where the total cavity length L is 1 463.518 μm. From (2), it can be seen that the change in the cavity length is proportional to the temperature change, so that temperature measurement can be realized by determining the cavity length. In this article, a cross-correlation method [33] for absolute cavity length demodulation is used, which is a spectral-domain demodulation technique, to achieve sub-nanometer high-resolution demodulation of the absolute cavity length of the fiber FPI sensor.

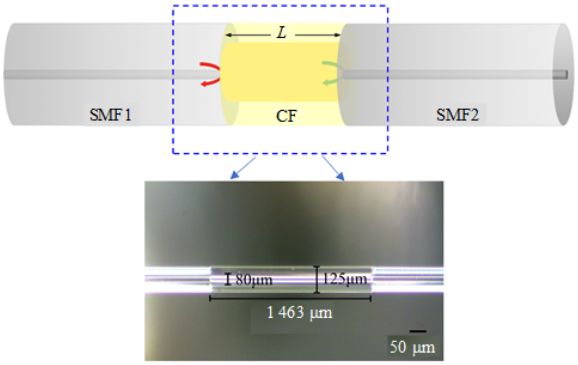

Fig. 1 Schematic diagram of the proposed FPI sensor.

We next provide an estimation of the temperature response time of the FPI sensor. The proposed FPI sensor can be considered to have a single-layer cylindrical structure with a uniform temperature distribution, which indicates that the heat transfer process can be briefly analyzed with the lumped parameter model (LPM) [34]. This assumption is justified by the small Biot number, B_i, of the sensor in water. The Biot number is defined as

$$B_i = hL_c / K_s \tag{3}$$

where L_c is the characteristic length of the sensor structure, which is the wall thickness of the sensor in

this paper, defined as V_s/A_s, where V_s represents the volume of the sensor, A_s represents the surface area [35, 36], K_s is the heat conductivity of silica, and h is the heat transfer coefficient (HTC). A small Biot number ($\ll 1$) implies that the temperature is uniform throughout the object. Taking $h=422.2$ W/m^2 [22], $K_s=1.38$ W/(m·K) [37, 38], and $L_c \approx 22.5$ μm, it can be calculated that $B_i \approx 0.006$ for a capillary tube made of silica (the refractive index of 1.444 at 1 550 nm) with an inner diameter of 80 μm and an outer diameter of 125 μm. Hence, $B_i \ll 1$ verifies that the LPM can be employed for the sensor proposed here and used in water. Thus, the heat balance formula for isotropic solids can be expressed as the following equation [39]:

$$hA_s\left(T_\infty - T\right)\mathrm{d}t = \rho_s C_s V_s \mathrm{d}T \tag{4}$$

where T_∞ is the ambient temperature, T is the temperature of the sensor, and t is time, ρ_s and C_s are the material density and specific heat capacity, respectively.

We assume that the temperature of the sensor is T_0 at $t=0$. The relationship of the temperature of the sensor T at any time t during the heat exchange process can be obtained by [40]:

$$(T-T_\infty)/(T_\infty - T_0) = -\exp\left(-t/\tau\right) \tag{5}$$

where

$$\tau = \rho_s C_s V_s / (hA_s) \tag{6}$$

is the time constant that is defined as the response time, e.g., the time required for the sensor to register 63.2% of the change at the temperature [22]. It is worth exploring the dependence of the response time on the fiber diameter, which can be calculated by the following transformation of (6):

$$\tau = \rho_s C_s V_s / (hA_s) = \rho_s C_s r/(2h) = \rho_s C_s d/(4h) \tag{7}$$

where r is the fiber radius and d is the fiber diameter. Equation (7) indicates that smaller-diameter silica has shorter response time.

3. Structure and wavelength tuning mechanism of MG-Y laser

The reflection spectrum of the FPI sensor needs to be acquired quickly for rapid temperature measurement. In the past few years, MG-Y semiconductor lasers have been widely studied as important components of optical communications systems for their fast wavelength tuning speed. Thanks to this advantage, MG-Y lasers combined with the homemade hardware and software offer the rapid continuous real-time in situ measurement potential for temperature sensing. Figure 2(a) illustrates a simplified structure diagram of the MG-Y tunable laser. The laser has a right Bragg reflector and a left Bragg reflector, a multimode interferometer (MMI) that combines the beams coming from the two Bragg reflectors, a phase section, a gain section, and a semiconductor optical amplifier (SOA) reflector.

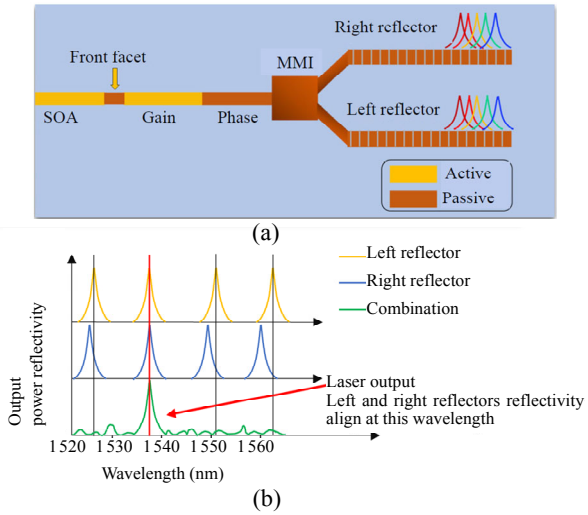

Fig. 2 Schematic structure and tuning mechanism of the MG-Y tunable laser: (a) simplified scheme of the MG-Y tunable laser and (b) intensity reflectance spectrum of both Bragg reflectors and their combination.

A periodic grating produces a comb-like spectrum [41] in each Bragg reflector, with the Bragg wavelength evenly spaced. The MMI section connects the reflectance of two Bragg reflectors to generate an additive combination. The spectrum of the Bragg reflectors and their combination is shown in Fig. 2(b). The reflection peaks separations of the Bragg reflectors are made slightly different so that only one peak of each reflector overlaps for any wavelength shift, which is called the Vernier effect [42]. The reflection peaks can be tuned by injecting

currents into the Bragg reflectors, so the combined reflection peak can be adjusted accordingly. To achieve improved tuning precision and allow the continuous wavelength tuning, the current is injected into the phase section facilitating fine resonant wavelength adjustments by altering the effective cavity length [43]. Both the Bragg reflectors and the phase section adjustment yield a broad and continuous tuning range with a relatively low injection current.

4. Design details of the homemade interrogator based on MG-Y laser

The schematic setup of the temperature measurement system with the MG-Y tunable laser is shown in Fig. 3(a). The entire system can be divided into three parts: the MG-Y laser, electrical modules, and the FPI sensor. A field-programmable gate array (FPGA) chip is exploited as the central controller of the interrogator. The printed circuit board (PCB) contains five digital-to-analog converters (DACs) with the capability of producing 0 mA–300 mA, respectively, which is sufficient to drive the MG-Y laser. A temperature controller (ADN8834 provided by Analog) can provide a maximum current of 1.5 A for the thermoelectric cooler (TEC), which can be used as a temperature control module for the MG-Y laser. The electrical module also contains a photodiode (PD) with the responsivity of 0.8 A/W, a linear amplifier, an analog-to-digital conversion (ADC) module with the 12-bit resolution, and a universal serial bus (USB) port. Figure 3(b) shows the custom-fabricated PCB of the interrogator based on the MG-Y laser. A look-up table (LUT) containing the relationship between a set of laser wavelengths and their corresponding currents combinations is stored in the FPGA flash memory, which allows the wavelength to be tuned over the entire spectrum from 1 527 nm–1 567 nm with the 8-pm step. Light from the MG-Y laser passes an optical circulator and then is incident into the FPI sensor; the reflected light from the sensor is then received by the PD; the resultant signal is amplified and converted digitally, and then is sent to the FPGA through the USB port. Finally, the FPGA transfers the relevant information to the computer for further digital signal processing.

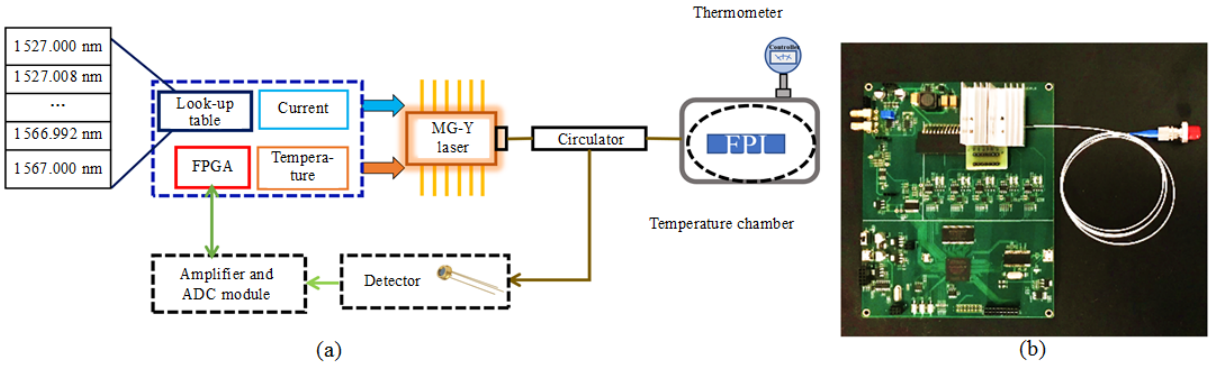

Fig. 3 Experimental setup for the temperature measurement: (a) schematic setup of the FPI temperature sensing system based on the MG-Y laser and (b) the custom-fabricated printed circuit board of the homemade interrogator based on the MG-Y laser.

4.1 MG-Y laser, near infrared (NIR) detector, and ADC

The MG-Y laser (ATLS7500, AOC Technology) used in this system is a butterfly-packaged fiber-coupled tunable laser covering the entire C-band wavelength range from 1 527 nm–1 567 nm. A negative temperature coefficient (NTC) thermistor is adopted to measure the internal temperature of the laser, based on which the current passing through the TEC controller is adjusted in real time to stabilize the laser temperature. The output wavelength can be tuned by changing the currents of the left and right reflectors, and the phase sections,

while the output power of the laser is changed by adjusting the injection current of the SOA and the gain sections. Besides, this system incorporates an InGaAs photodiode (LSIPD-A75, Beijing Lightsensing Technologies Ltd.) intended for photoelectric conversion, and an AD9226 unit with a high sampling rate of 65 MSPS and 12-bit resolution, which enables highspeed interference spectrum collection.

4.2 Laser driver module

With the capability of delivering up to a 300-mA stable current with the low noise and long-term stability, the ADN8810 is a 12-bit current source suitable to drive the tunable lasers that require low-noise precise current sources. The ADN8810 chip and peripheral control circuit are used to comprise the current driver, which can provide currents for the left reflector, right reflector, phase section, gain section, and OA section of the MG-Y laser, respectively. Furthermore, the maximum current can be adjusted to meet the needs of various laser current drivers by changing the external resistance within a certain range.

It is necessary to impose the temperature control on the MG-Y laser because the wavelength shows the greater sensitivity to the variation of the temperature than that of the current [44]. Therefore, maintaining the stable operation temperature of the laser plays a vital role in ensuring consistent output wavelengths. By taking advantage of the Peltier effect, the temperature of the laser can be controlled by the TEC module. The temperature can be monitored in real time by the inbuilt thermistor with a negative temperature coefficient (NTC). We use a highly integrated TEC controller based on ADN8834 to control the laser temperature. The laser temperature is maintained by an analog proportion-integral-differential (PID) control loop circuit involving the NTC thermistor.

5. Validation of instrument function

Instead of using the traditional electrical method, some optical methods are adopted in this study to evaluate the performance of our system.

The major evaluation criterion is the wavelength profile of the laser output as acquired by the multi-wavelength meter (Yokogawa, AQ6151).

5.1 Effect of injection current on wavelength in different sections of the laser

We first explore the impact of injection current in different sections on the wavelength of the laser. The tuning characteristics of the left and right reflectors are analyzed, with the initial output power of about 10 dBm by maintaining the currents in the gain section and SOA section with $I_{GAIN}=98$ mA and $I_{SOA}=100.76$ mA, respectively. Meanwhile, the laser is maintained at a constant temperature of 25 ℃. The map of laser wavelengths as a function of the right and left reflector currents is obtained by tuning the currents I_{RR} and I_{LR} separately from 0 mA to 20 mA with the step of 0.2 mA, while the phase section current is kept at $I_{phase}=0$ mA. As shown in Fig. 4(a), there are 11 pathways in total. From them, 100 wavelengths with a high side-mode suppression ratio (SMSR) are selected, covering a wide range from 1 527 nm to 1 567 nm with an interval of 0.4 nm, as shown in Fig. 4(b).

Next, only the phase section current is adjusted to analyze the characteristics of wavelength fine-tuning around certain wavelengths in the map. During the experiment, the currents of the left and right reflectors remain unchanged, but the phase section current I_{phase} varies from 0 mA to 5 mA, with a scanning step size of 0.1 mA. By adjusting the current passing through the phase section, two wavelengths $\lambda_1=1\,530.966\,1$ nm ($I_{RR}=2.385$ mA and $I_{LR}=6.121$ mA) and $\lambda_2=1\,550.753\,9$ nm ($I_{RR}=3.624$ mA and $I_{LR}=1.706$ mA) are selected to explore the characteristics of wavelength fine-tuning.

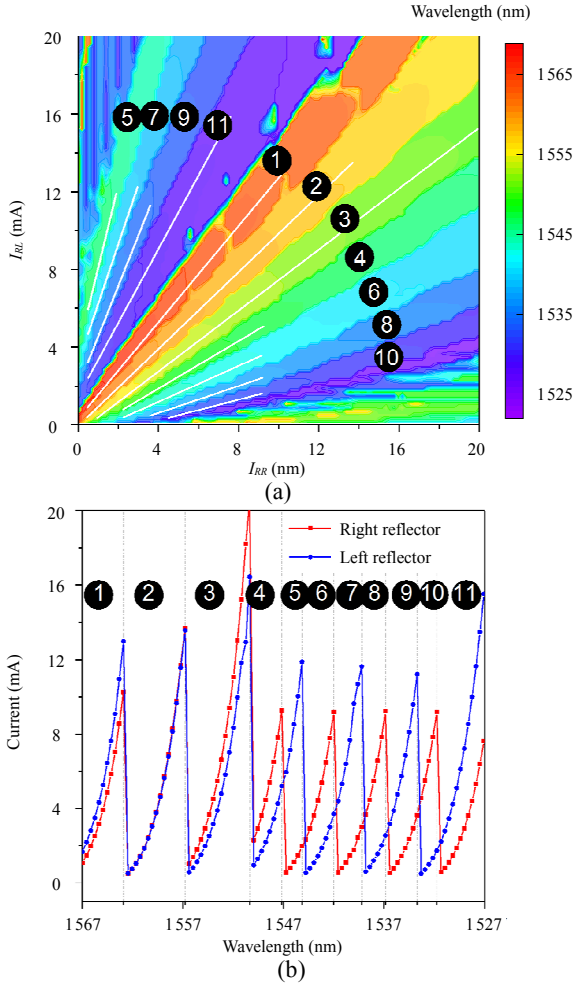

Fig. 4 Typical map of tuned wavelength covering a range of 40 nm: (a) relationship among the eleven tuning paths, I_{RR} and I_{LR} and (b) current tuning paths of I_{RR} and I_{LR} with 0.4 nm wavelength interval.

As shown in Fig. 5(a), mode hopping is preceded by a segment of a linear curve with a wavelength fine-tuning span of approximately 0.3 nm. The tuned wavelength, in particular, is negatively proportional to I_{phase}, showing a good linearity across this span, which is helpful in achieving high-resolution wavelength tuning. Another characteristic of the MG-Y laser is that the output power of the laser depends on the current applied to the SOA section. Since the flat output power of a tunable laser is required for various optical sensing techniques, including FPI sensors and FBG sensors, it is necessary to obtain a relationship between the SOA section current and the output power of the laser. There are eight wavelengths selected to investigate the SOA section current versus the output power, 1 529.408 nm, 1 532.915 nm, 1 537.631 nm, 1 542.772 nm, 1 547.948 nm, 1 557.589 nm, 1 563.680 nm, and 1 567.768 nm. Figure 5(b) shows the corresponding power changes versus the SOA current, showing an approximately linear relationship between the applied current and the output power, when the current in the SOA section varies from 70 mA to 160 mA. With the above measurement, a flat output power of different wavelengths of the laser can be achieved by adequately adjusting the SOA current. In our system, the laser is calibrated to the output power of 10 dBm, meeting the requirements of fiber-optic sensing.

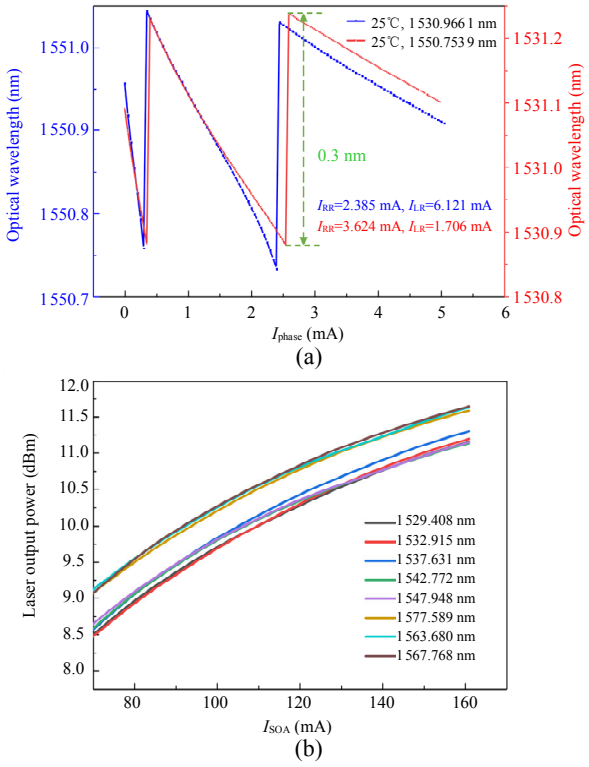

Fig. 5 Effect of injection current values in phase and SOA regions on the MG-Y laser: (a) characteristics of phase-area current tuning and (b) SOA curves for MG-Y laser. The injection current ranges from 70 mA to 160 mA.

Finally, the linear fine-tuning is performed by sweeping the phase region current, the output power of a tunable laser is calibrated, and a fine LUT with the high resolution of 8 pm is created. As shown in Fig. 6, our system achieves a wavelength tuning

range from 1 527 nm to 1 567 nm, and the full-spectrum measurement rate reaches 100 Hz.

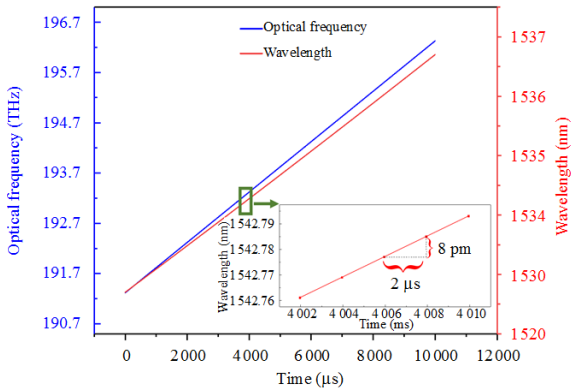

Fig. 6 LUT with 8-pm resolution and the total scanning time for the C-band wavelength of 10 ms.

5.2 Stability of the temperature

Temperature stability is an important parameter required to assess the performance of the laser driver. To characterize the long-term stability of temperature, 25 ℃ is set as the test temperature. A multimeter (Agilent, 34405A) is used to monitor the voltage across a thermistor inside the MG-Y laser. The resistance value of the thermistor is obtained by calculating the voltage to determine the actual temperature of the MG-Y laser. Figure 7 shows temperature drift from the set temperature for several hours. The maximum temperature change (the highest and the lowest temperatures) is less than 0.002 3 ℃ for the MG-Y laser, suggesting that the MG-Y laser can be maintained at a constant temperature with the temperature controller in use.

When the temperature changes, the emission wavelength of the MG-Y laser varies. To further reveal the relationship between the wavelength drift and laser temperatures, the temperature is set to the range from 20 ℃ to 30 ℃ with a 1 ℃ increment, with 10-second dwelling time at each temperature.

Then, the wavelength is plotted as a function of the temperature, and an excellent linear relationship between the wavelength and the temperature is obtained as shown in Fig. 8. Based on linear fitting, the correlation coefficient is calculated to be 0.996, suggesting a good linear relationship between the output wavelength of the MG-Y laser and temperature variation.

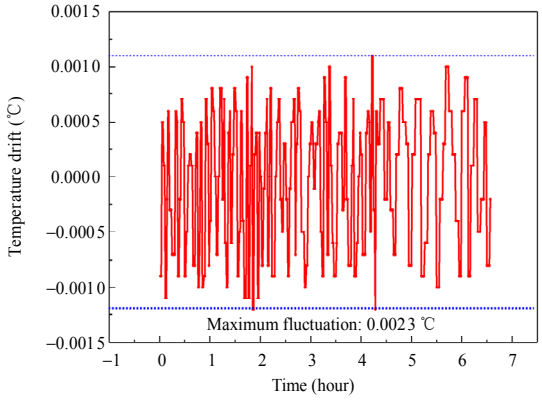

Fig. 7 Temperature drift of the MG-Y laser. The working temperature at 25 ℃ is shown as a function of time and the test lasts 6.5 hours.

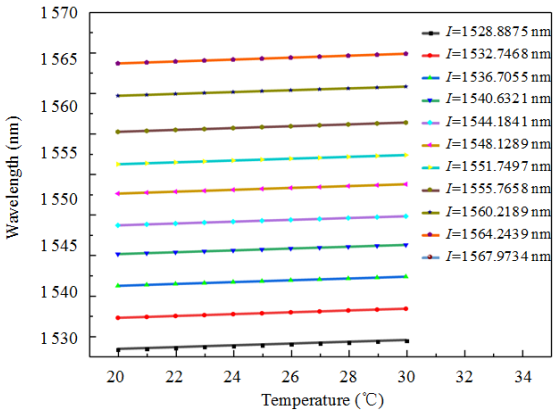

Fig. 8 Linearity of wavelength given different injection currents and working temperatures.

5.3 Noise and stability of wavelength

To assess the short-term stability, the MG-Y laser is operated for 600 s consecutively under the constant current and temperature. The wavelength data are collected using a multi-wavelength meter with a maximum sampling frequency of 5 Hz. Then, the data are transferred to the computer via the Ethernet interface. To verify the short-term stability of the system, the laser is set to a wavelength of 1 529.392 7 nm at 20 ℃ and 1 567.738 1 nm at 30 ℃. As shown in Fig. 9, the maximum wavelength drift is less than 0.4 pm. The temperature is kept constant throughout the experiment at the preset point with the temperature control module.

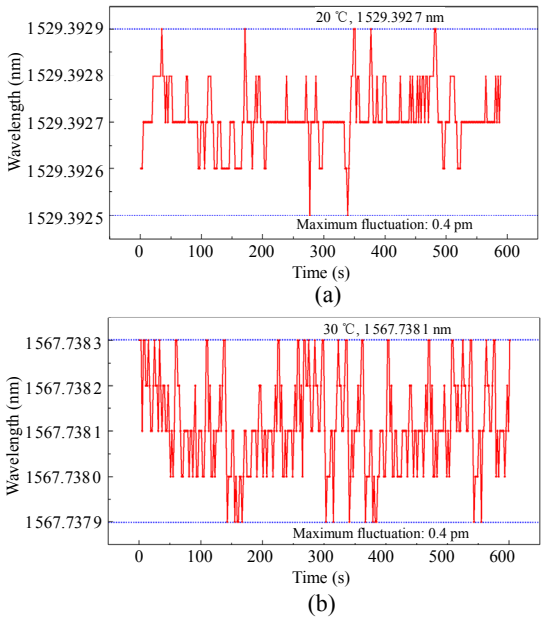

Fig. 9 Short-term stability of the laser output beam under constant current and temperature: (a) the temperature is 20 ℃ and the wavelength of the MG-Y laser is 1 529.392 7 nm and (b) the temperature is 30 ℃ and the wavelength of the MG-Y laser is 1 567.738 1 nm.

The system's long-term stability is evaluated by conducting a wavelength drift experiment for approximately 6 days to demonstrate the instrument's consistent performance further. We select 4 representative wavelengths in the same experimental environment (25 ℃). Each wavelength is output 10 000 times, respectively, and the corresponding wavelength result is collected every 15 s, so each wavelength is tested for one and a half working days to test the stability of its wavelength output. The wavelength fluctuation curve with the sampling number is shown in Fig. 10. The maximum drift of the wavelength in the four test datasets is about 1 pm. Laser wavelength fluctuations come from the instabilities in the temperature controller and the current driver itself. In future work, we will design a higher precision current driver to improve the system's stability.

Finally, an FPI sensor is constructed and the cavity length is measured to be roughly 535 μm using a commercial interrogator (sm125, Micron Optics). The interference spectrum is captured by the homemade interrogator to evaluate the performance of the system further. According to the spectrum of the sensor shown in Fig. 11, the total cavity length obtained by the cross-correlation algorithm is 535.105 μm, which confirms the feasibility of the system.

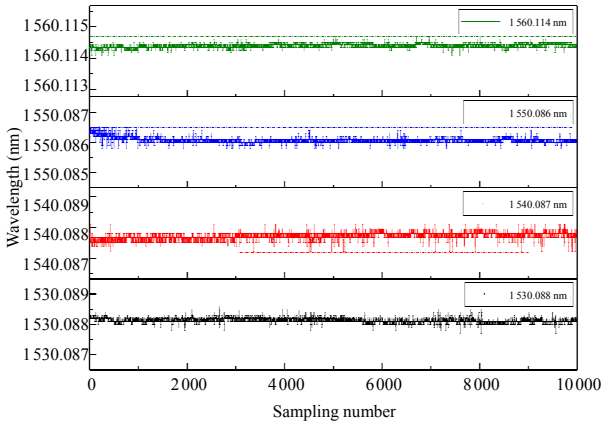

Fig. 10 Long-term drift of the laser output beam under constant current and temperature.

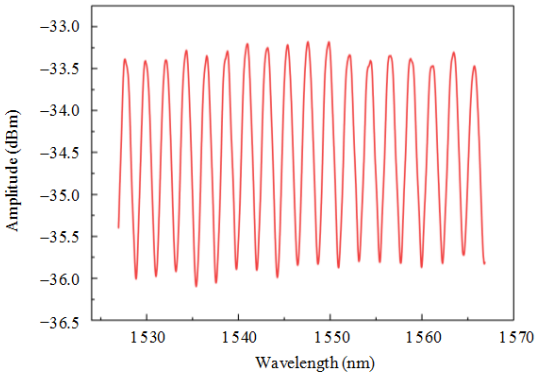

Fig. 11 Frame of the reflection spectrum measured by the homemade interrogator.

6. Experiments and discussion

6.1 Static temperature experiment

In order to verify the temperature measurement system, the FPI sensor is made by splicing a section of a hollow capillary tube between two pieces of SMFs with a total cavity length of approximately 1 463 μm. Besides, the FPI sensor is placed in the heating chamber with a temperature range of 0 ℃–250 ℃ and the precision of 0.1 ℃. At the time of temperature ramping, the FPI sensor interference spectrum is collected at an increment of 15 ℃ in the range of 30 ℃–120 ℃, with the measurement

performed at each temperature which is held for 5 min to ensure temperature stabilization. Figure 12 shows the spectrum measured by the self-developed interrogator. The sensitivity result of the FPI sensor is shown in Fig. 13(a), indicating the cavity length as a function of temperature. The temperature sensitivity coefficient of the sensor is approximately 802 pm/℃. The temperature sensitivity coefficient is determined by the initial cavity length L and the coefficient of thermal expansion of the hollow capillary tube. The temperature sensitivity coefficient of the sensor can be changed by adjusting the cavity length. According to (2), the theoretical value of the temperature sensitivity coefficient approaches 805 pm/℃, when the initial cavity length is 1 463 μm. The experimental results are consistent with the results of theoretical calculation.

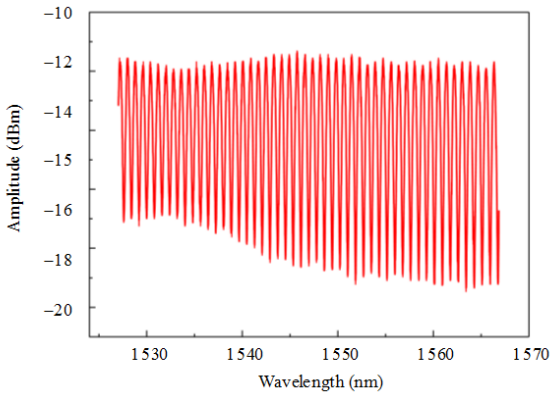

Fig. 12 Reflection spectrum of the sensor.

Afterwards, the temperature drops from 120 ℃ to 30 ℃ with a step of 15 ℃, and the sensitivity measurement results are also shown in Fig. 13(a). According to the experimental results, the FPI sensor shows clearly a linear relationship between the cavity length and the temperature, which confirms the applicability of the interrogator and the FPI sensor in temperature monitoring. The resolution is obtained by measuring the standard deviation of the cavity length of the FPI sensor over a certain period of time. The real-time cavity length is recorded once per second at room temperature for 10 min. The results of cavity length measurement are shown in Fig. 13(b), which shows the standard deviation of about 0.121 nm. We define the resolution of the cavity length of the proposed sensor to be twice the measurement standard deviation [33], so the demodulation resolution of the cavity length is about 0.242 nm, and the temperature resolution of the proposed sensor is about 0.302 ℃.

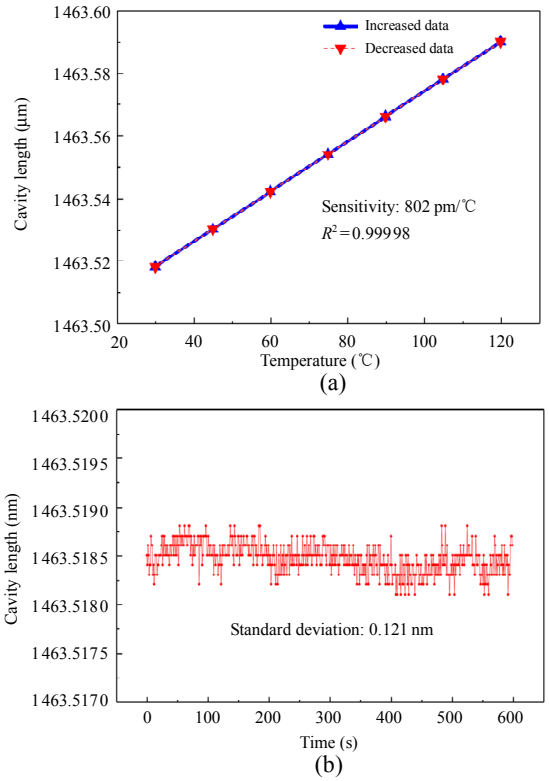

Fig. 13 Temperature response of the all-fiber FPI sensor: (a) cavity length-temperature variation curve of the FPI sensor and (b) variations of the FPI cavity length over time at room temperature.

6.2 Response time

In this section, the dynamic response of the temperature sensor is analyzed in water mediums, where the temperature sensor experiences a step temperature change. The cross-correlation algorithm is used to measure the cavity length of the FPI sensor rapidly. According to (7) and the theoretical results shown in Fig. 14(a), the silica tube with a smaller diameter leads to a faster response. As shown in Fig. 14(b), the proposed sensor made of silica with an inner diameter of 80 μm and an outer diameter of 125 μm has the response time of 92 ms.

To conduct a dynamic temperature experiment,

the sensor is immersed just below the water's surface in a container at room temperature and the volume of cold water is relatively small. The sensor is placed just below the surface of the water, so as to make the added hot water and the cold water around the sensor mix rapidly, making the temperature change of the sample more obvious. Then by pouring hot water into the container, the water temperature is changed suddenly, as shown in Fig. 15(a). Due to the heat transfer between the sensor head and the hot water, the cavity length elongates, as monitored by the interrogator, with a measuring frequency of 100 Hz. Figure 15(b) shows the cavity length of the sensor as a function of time.

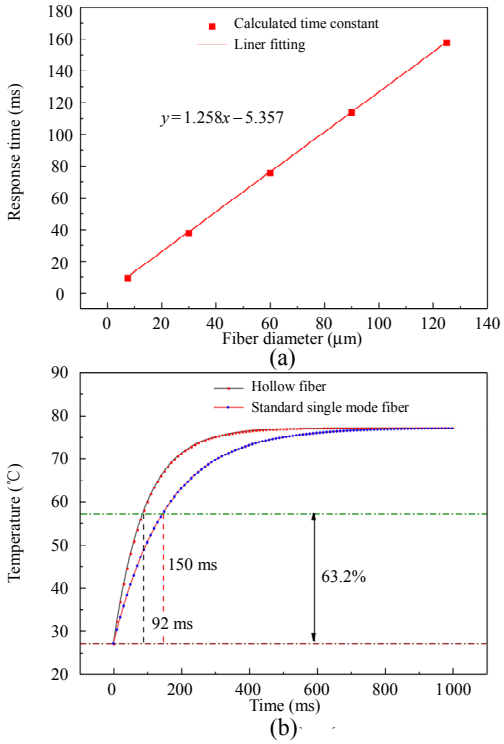

Fig. 14 Theoretical calculation of response time of all-fiber FPI sensors with different structures: (a) dependence of response time on fiber diameter and (b) simulated temperature over time for hollow and solid fiber.

As shown in Fig. 15(b), the 63.2% rise time is found to be 91.6 ms, which is basically consistent with the theoretical prediction shown in Fig. 14(b). Finally, we also test the reverse response of the temperature sensor by repeatedly immersing and removing the FPI sensor from hot water. As shown in Fig. 16, the response time is roughly 94 ms. However, the response time is slightly different at each time, e.g., 94 ms and 96 ms, which is mainly due to different rates at which the sensor drops from air to hot water [22]. There are two inflection points A and B found on the cooling curve; this is due to the fact that when the FPI sensor is removed from the hot water, there is a small amount of water adhering to the sensor itself and absorbing heat from the air due to evaporation, thus causing the temperature of the sensor to fall below the room temperature.

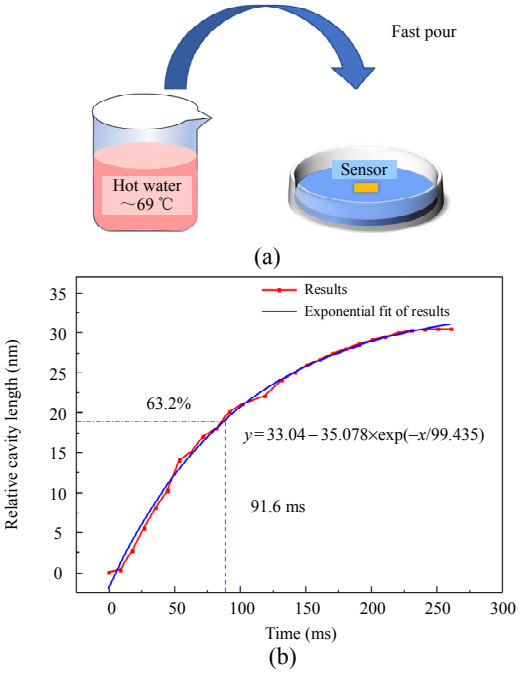

Fig. 15 Measurement of temperature response time: (a) response time is measured by the rapid immersion in hot water and (b) experimental relative cavity length versus time.

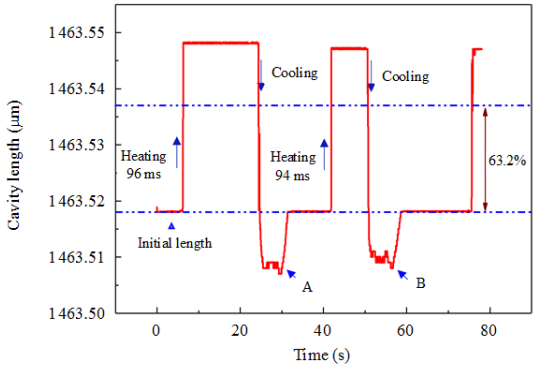

Fig. 16 Response time of the FPI sensor with the interrogator by immersing and removing the sensor from the hot water to cold air repeatedly.

7. Conclusions

In summary, a cost-effective and miniaturized instrument based on the MG-Y laser is developed for rapid temperature measurement by using the FPI sensor in this study. The homemade laser controller is demonstrated to have such advantages as high short-term and long-term stability, low noise, and the good linear response to ensure the effective operation of the MG-Y laser. The interference signal interrogator based on the MG-Y laser is developed with the homemade current driver and temperature controller to capture a wide range interference spectrum from 1 527 nm to 1 567 nm with the resolution of 8 pm. The sensor with a 1 463-μm cavity length has the temperature measurement sensitivity of 802 pm/℃, and the response time of 94 ms. The whole system has the potential of application for fast temperature measurement in harsh conditions.

Acknowledgment

This work was supported by the National Natural Science Foundation of China (Grant No. 62271101) and the Fundamental Research Funds for Central Universities (Grant No. DUT21ZD212).

Declarations

Conflict of Interest The authors declare that they have no competing interests.

References

[1] J. Q. Feng, P. Sun, W. H. Tang, D. P. Buse, Q. H. Wu, Z. Richardson, *et al*., "Implementation of a power transformer temperature monitoring system," in *Proceedings. International Conference on Power System Technology. IEEE*, China, 2002, pp. 1980–1983.

[2] J. Kortschinski and J. R. Leslie, "A power-cable temperature monitoring system," *IEEE Transactions on Power Apparatus and Systems*, 1970, PA89(7): 1429–1433.

[3] E. M. Saber, K. W. Tham, and H. Leibundgut, "A review of high temperature cooling systems in tropical buildings," *Building and Environment*, 2016, 96: 237–249.

[4] P. J. Tannous, S. R. T. Peddada, J. T. Allison, T. Foulkes, R. C. N. Pilawa-Podgurski, and A. G. Alleyne, "Dynamic temperature estimation of power electronics systems," in *IEEE 2017 American Control Conference*, Seattle, USA, 2017, pp. 3463–3469.

[5] I. Fofana and Y. Hadjadj, "Electrical-based diagnostic techniques for assessing insulation condition in aged transformers," *Energies*, 2016, 9(9): 679.

[6] W. Hou, G. Liu, and M. Han, "A novel, high-resolution, high-speed fiber-optic temperature sensor for oceanographic applications," in *2015 IEEE/OES 11th Current, Waves and Turbulence Measurement*, St. Petersburg, USA, 2015, pp. 1–4.

[7] G. Liu, M. Han, W. Hou, S. Matt, and W. Goode, "A miniature fiber-optic sensor for high-resolution and high-speed temperature sensing in ocean environment," *Proceedings of SPIE: Ocean Sensing and Monitoring VII*, 2015, 9459: 80–85.

[8] G. Liu, Q. Sheng, W. Hou, M. L. Reinke, and M. Han, "A silicon-tipped fiber-optic sensing platform with high resolution and fast response," *Journal of Visualized Experiments*, 2019, 143: e59026.

[9] Z. Liu, "Investigation of silicon-based microstructure Fabry-Perot interferometric optical fiber sensing technology," Ph.D. dissertation, Dalian University of Technology, Dalian, China, 2020.

[10] G. X. Ren, X. Y. Wang, and L. B. Du, "Design of high-precision and fast-response temperature measurement system for ocean," *Instrument Technique and Sensor*, 2011, 2: 25–47.

[11] C. S. Monteiro, A. Vaz, D. Viveiros, C. Linhares, S. M. O. Tavares, H. Mendes, *et al*., "FBG two-dimensional vibration sensor for power transformers," *Proceedings of SPIE: 7th European Workshop on Optical Fibre Sensors*, 2019, 11199: 105–108.

[12] Y. Li, G. Yan, L. Zhang, and S. He, "Microfluidic flowmeter based on micro "hot-wire" sandwiched Fabry-Perot interferometer," *Optics Express*, 2015, 23(7): 9483–9493.

[13] K. Li, J. Xin, F. Luo, and L. Zhu, "Central wavelength interrogation method of ultra-short FBG by dual-wavelength laser," *Laser & Optoelectronics Progress*, 2018, 55(3): 030602.

[14] X. Liu, Q. Li, Y. Zhang, and S. Zhou, "Research of temperature response time hysteresis rule on fiber

Bragg grating sensing," *Optical Technique*, 2014, 40: 156–159.
[15] D. Zhang, J. Wang, Y. Wang, and X. Dai, "A fast response temperature sensor based on fiber Bragg grating," *Measurement Science and Technology*, 2014, 25(7): 075105.
[16] H. Meng, H. Y. Li, and Z. Q. Cao, "An optical fiber Farby-Perot temperature sensor for rapid ocean temperature measurement," *Chinese Journal of Lasers-Zhongguo Jiguang*, 2018, 45(12): 256–260.
[17] Y. N. Zhang, L. Yuan, X. W. Lan, A, Kaur, J. Huang, and H. Xiao, "High-temperature fiber-optic Fabry-Perot interferometric pressure sensor fabricated by femtosecond laser," *Optics Letters*, 2013, 38(22): 4609–4612.
[18] G. Liu, Q. Sheng, G. R. L. Piassetta, W. Hou, and M. Han, "A fiber-optic water flow sensor based on laser-heated silicon Fabry-Pérot cavity," *Proceedings of SPIE: Fiber Optic Sensors and Applications XIII*, 2016, 9852: 288–294.
[19] C. Zhu, R. E. Gerald, and J. Huang, "A dual-parameter internally calibrated Fabry-Perot microcavity sensor," *IEEE Sensors Journal*, 2020, 2(5): 2511–2517.
[20] F. Zhao, J. Wang, Y. Xiao, K. Zhang, R. Chen, and S. Liu, "Curvature monitoring of power grid wires based on anti-resonant reflecting guidance in hollow core fibers," *Optik*, 2020, 213: 164785.
[21] N. Cai, L. Xia, and Y. Wu, "Multiplexing of anti-resonant reflecting optical waveguides for temperature sensing based on quartz capillary," *Optics Express*, 2018, 26(25): 33501–33509.
[22] J. H. Wen, J. Wang, L. Yang, Y. F. Hou, D. H. Huo, E. L. Cai, *et al.*, "Response time of microfiber temperature sensor in liquid environment," *IEEE Sensors Journal*, 2020, 20(12): 6400–6407.
[23] X. Zhou and Q. Yu, "Wide-range displacement sensor based on fiber-optic Fabry-Perot interferometer for subnanometer measurement," *IEEE Sensors Journal*, 2011, 11(7): 1602–1606.
[24] H. Chen, J. Liu, X. Zhang, W. Wang, Z. Ma, W. Lv, *et al.*, "High-order harmonic-frequency cross-correlation algorithm for absolute cavity length interrogation of white-light fiber-optic Fabry-Perot sensors," *Journal of Lightwave Technology*, 2020, 38(4): 953–960.
[25] J. Wang, Y. P. Liao, S. S. Wang, and X. Wang, "Ultrasensitive optical sensing in aqueous solution based on microfiber modal interferometer," *Optics Express*, 2018, 26(19): 24843–24853.
[26] S. W. Lloyd, J. A. Newman, D. R. Wilding, R. H. Selfridge, and S. M. Schultz, "Compact optical fiber sensor smart node," *Review of Scientific Instruments*, 2007, 78(3): 035108.
[27] J. Liu, L. Zhu, W. He, Y. Yang, F. Meng, and Y. Song, "Fiber grating sensing interrogation system based on a modulated grating Y-branch tunable laser for core-and-cladding- integrated fiber Bragg grating temperature measurement," *Review of Scientific Instrument*s, 2020, 91(1): 014904.
[28] Y. Cheung, Z. Jing, A. Li, Q. Liu, Y. Liu, Z. Huang, *et al.*, "An integrated fiber-optic white-light interferometry system based on VT-DBR laser," in *IEEE 2021 19th International Conference on Optical Communications and Networks*, China, 2021, pp. 1–3.
[29] Y. Liu, Z. Jing, Q. Liu, A. Li, A. Lee, Y. Cheung, *et al.*, "All-silica fiber-optic temperature-depth-salinity sensor based on cascaded EFPIs and FBG for deep sea exploration," *Optics Express*, 2021, 29(15): 23953–23966.
[30] H. Wu, Q. Meng, J. Li, B. Han, Z. Wang, Y. Rao, *et al.*, "Spectral tailoring of random fiber laser based on the multimode interference filter," *IEEE Access*, 2018, 6: 39435–39441.
[31] K. Iga, "Forty years of vertical-cavity surface-emitting laser: invention and innovation," *Japanese Journal of Applied Physics*, 2018, 57(8S2): 08PA01.
[32] D. Derickson, M. Bernacil, A. DeKelaita, B. Maher, S. O'Connor, M. N. Sysak, *et al.*, "SGDBR single-chip wavelength tunable lasers for swept source OCT," *Proceedings of SPIE: Coherence Domain Optical Methods and Optical Coherence Tomography in Biomedicine XII*, 2008, 6847: 392–402.
[33] Y. Liu, Z. Jing, R. Li, Y. Zhang, Q. Liu, A. Li, *et al.*, "Miniature fiber-optic tip pressure sensor assembled by hydroxide catalysis bonding technology," *Optics Express*, 2020, 28(2): 948–958.
[34] G. Liu, M. Han, and W. Hou, "High-resolution and fast-response fiber-optic temperature sensor using silicon Fabry-Pérot cavity," *Optics Express*, 2015, 23(6): 7237–7247.
[35] A. Faghri, Y. Zhang, and J. R. Howell, "*Advanced Heat and Mass Transfer*," Columbia: Global Digital Press, 2010.
[36] M. Akbari, R. Abdi Behnagh, and A. Dadvand, "Effect of materials position on friction stir lap welding of Al to Cu," *Science and Technology of Welding and Joining*, 2012, 17(7): 581–588.
[37] B. Ryningen, M. Bellmann, R. Kvande, and O. Lohne, "The effect of crucible coating and the temperature field on minority carrier lifetime in directionally solidified multicrystalline silicon ingots," in *Proceedings of the 27th European Photovoltaic Solar Energy Conference and Exhibition*, Germany, 2012, pp. 24–28.
[38] S. Reynolds, Material of the month: fused silica [Online]. Available, https://www.swiftglass.com/blog/material-month-fused-silica/, April 2017.
[39] M. Ding, P. Wang, and G. Brambilla, "Fast-response high-temperature microfiber coupler tip thermometer," *IEEE Photonics Technology Letters*, 2012, 24(14): 1209–1211.

[40] P. Rinaudo, I. Paya-Zaforteza, P. Calderón, and S. Sales, "Experimental and analytical evaluation of the response time of high temperature fiber optic sensors," *Sensors and Actuators A: Physical*, 2016, 243: 167–174.

[41] M. C. Bustillos-Barcaya, G. F. Rinalde, L. A. Bulus-Rossini, and P. A. Costanzo-Caso, "Y-branch tunable laser design: modeling, control and experimental validation," *Optics & Laser Technology*, 2021, 140: 107040.

[42] M. Chacinski, M. Isaksson, and R. Schatz, "High-speed direct Modulation of widely tunable MG-Y laser," *IEEE Photonics Technology Letters*, 2005, 17(6): 1157–1159.

[43] M. Lewander, A. Fried, P. Weibring, D. Richter, S. Spuler, and L. Rippe, "Fast and sensitive time-multiplexed gas sensing of multiple lines using a miniature telecom diode laser between 1529 nm and 1565 nm," *Applied Physics B*, 2011, 104(3): 715–723.

[44] N. Li, X. Qiu, Y. Wei, E. Zhang, J. Wang, C. Li, *et al*., "A portable low-power integrated current and temperature laser controller for high-sensitivity gas sensor applications," *Review of Scientific Instruments*, 2018, 89(10): 103103.